Field Stabilization with Post Couplers for DTL tank1 of Linac4

N. Alharbi, F. Gerigk, M. Vretenar

CERN, Geneva, Switzerland

Abstract

In this paper we study the field stabilization with post couplers for the first Drift Tube Linac (DTL) tank of Linac4, a new proton linac aiming to replace the existing Linac2 at CERN. Instead of using a cold model to determine the dispersion curves of the TM_{01} band and the post coupler band, 3D electromagnetic field simulations with Microwave Studio are used for this task. Up to now these simulations were considered too time consuming because of the large number of coupled cells that have to be simulated. However, as we will show in this paper, the problem can be scaled down to reduce number of cells, which can then be analyzed by modern PCs within a reasonable time frame. By changing the length of the post couplers we find the point where modes merge (confluence) and by means of 3D field simulations we can thus study the conditions for field stabilization. The optimum post coupler radius is then determined using the tilt sensitivity technique.

1- Introduction

Alvarez DTLs operate in the zero mode resulting in the same direction of the electric field in all accelerating gaps as shown in Fig. 1 (a). Since the group velocity $v_g = \partial\omega/\partial k_z$ of this mode, which is proportional to the slope of the dispersion [see Fig. 2 (a)] curve, is zero, there is basically no energy propagation from one gap to the next [1] rendering the electric field distribution very sensitive to small frequency perturbations in the cells. For the π/2 mode on the other hand, the tangent on the dispersion curve becomes maximum, yielding a high group velocity and making this mode the most stable mode of operation for any cell-coupled accelerating structure. Since the π/2 mode would be very inefficient for acceleration [2], one tries to change the slope of dispersion curve at the location of the zero mode by introducing a 2nd resonator band which is then coupled to the TM_{01} band. This can be done by inserting short cylinders (the post couplers) in the horizontal plane placed in correspondences to the drift tube centers. The dispersion curve of the post coupler (PC) band is shown in Fig. 2 (b). The post couplers are then tuned such that the frequency stop band between the two dispersion curves becomes very small. Maximum stabilization is achieved at confluence for a vanishing stop band. Figure 3 illustrates that at confluence we now have a non-zero slope for the dispersion curve at the location of the accelerating mode.

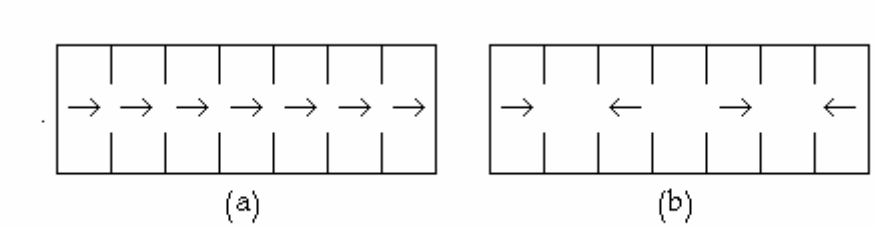

Figure 1: (a) electrical field of the zero mode (b) electrical field of the $\pi/2$ mode

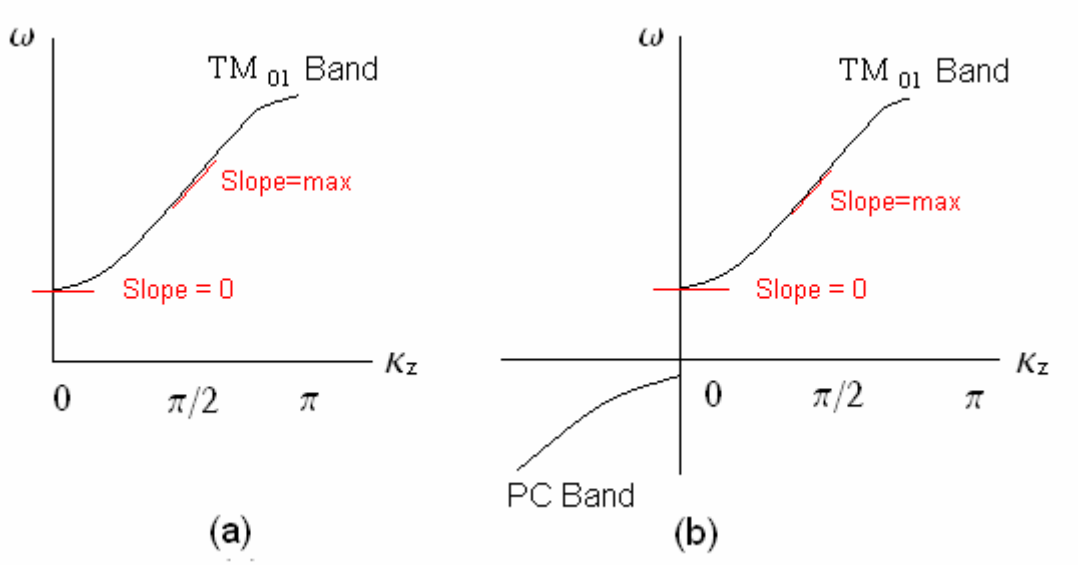

Figure 2: (a) shows the dispersion curve of TM_{01} band. The slope at zero mode point is zero. (b) shows the dispersion curves of TM_{01} band and PC band. The slope at zero mode point is still zero and there is a large stop band.

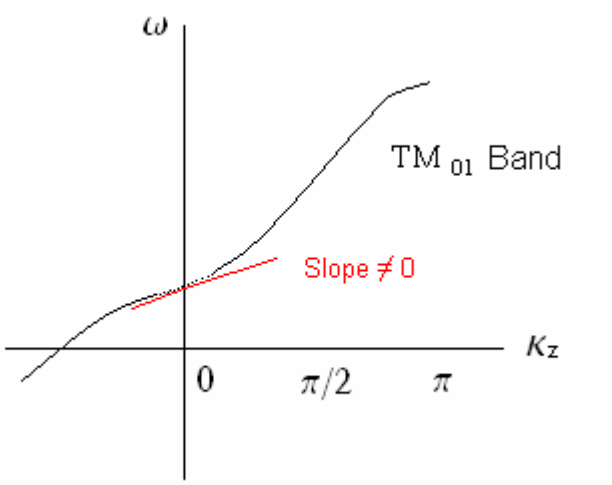

Figure 3: shows the dispersion curves of TM_{01} band and PC band. The slope at zero mode point is non-zero when both bands come to confluence.

2- Tank1

The DTL [3] of Linac4 [4] consists of three standard Alvarez tanks. Tank1 (see Fig. 4) accelerates the beam from a starting energy of 3 MeV to 9.8 MeV. It is composed of 28 drift tubes which increase in length according to the increase in particle energy. The tank itself has a length of 2.63 m and a diameter of 520 mm.

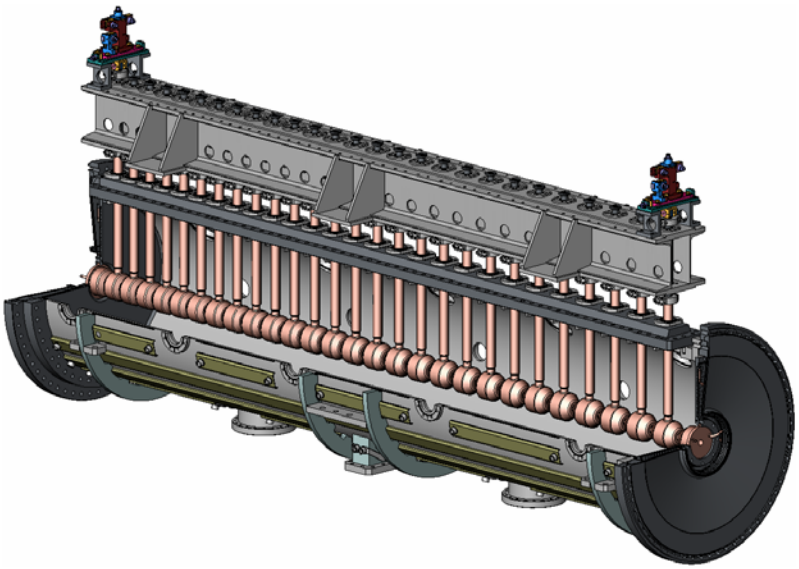

Figure 4: Longitudinal cut of Thank1 including the drift tubes

The general shape of a drift tube is shown in Fig. 5 and a list of all (changing) parameters for the drift tubes in Tank 1 is given in Table 1. The inner/outer nose radius, the corner radius and the length of the flat segment at the nose tip remain constant throughout Tank1 at 3 mm, 8 mm, 5 mm, and 9 mm, respectively. Using 2D simulations with Superfish these parameters were chosen to maximize the effective shunt impedance and to limit the peak electric field to 1.7 kilpatrick. In order to simplify the simulation model we use the geometry of the centre cell together with drift tube no. 14 for all simulated cells.

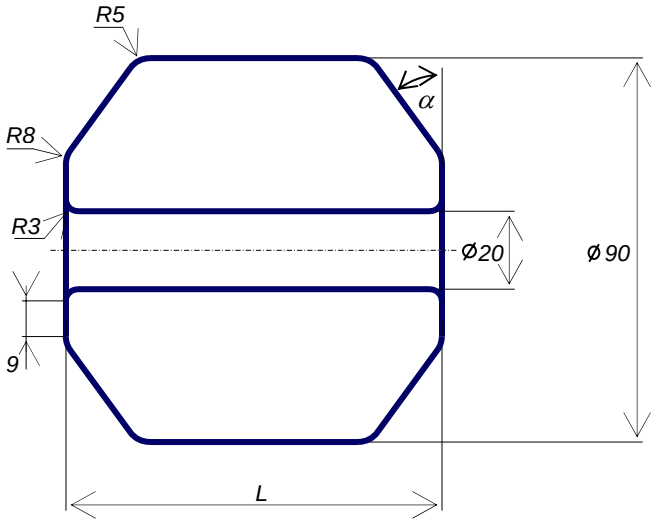

Figure 5: General geometry of drift tubes with constant values for the inner nose radius, outer nose radius and corner radius (3 mm, 8 mm and 5 mm)

No	Symmetric cell length, mm	Tube length, mm	Gap length, mm	Face angle α, deg	Asymmetric cell length, mm
0	0.000	29.992	0.000	25.105	0.000
1	68.729	60.734	8.744	25.970	69.104
2	70.447	62.214	8.963	26.835	70.437
3	72.188	63.698	9.244	27.895	72.201
4	73.953	65.217	9.500	29.085	73.957
5	75.740	66.750	9.760	30.355	75.743
6	77.549	68.299	10.029	31.615	77.554
7	79.379	69.867	10.301	32.930	79.384
8	81.228	71.452	10.573	34.365	81.232
9	83.098	73.053	10.850	35.795	83.102
10	84.986	74.670	11.128	37.300	84.990
11	86.892	76.315	11.411	39.050	86.903
12	88.817	77.971	11.668	40.905	88.811
13	90.757	79.762	11.965	44.085	90.831
14	92.716	81.414	11.985	45.405	92.574
15	94.690	83.012	12.592	46.385	94.805
16	96.678	84.672	12.753	48.120	96.594
17	98.680	86.248	13.262	48.680	98.721
18	100.694	87.908	13.617	50.165	100.694
19	102.721	89.534	13.982	51.215	102.703
20	104.759	91.068	14.429	51.790	104.730
21	106.657	92.601	14.851	52.385	106.685
22	108.707	94.186	15.311	53.015	108.705
23	110.760	95.759	15.784	53.580	110.757
24	112.816	97.326	16.274	54.145	112.816
25	114.874	98.164	16.764	54.290	114.509
26	115.076	99.985	16.859	54.980	115.933
27	119.701	102.202	17.949	56.465	119.043
28	120.930	51.326	18.277	57.950	120.705

Table 1: Drift tube and cell geometries for tank1

3- Dispersion Curve

The DTL tanks in Linac4 will be operate at a frequency of 352 MHz. The basic design was made with Superfish and 3D simulations with CST Microwave Studio (MWS) were employed to include features that break the 2D symmetry (drift tube stems, post couplers, tuners, etc). Fig. 6 shows the electric and magnetic fields of the simulation model for cell number 14 which is later on used to study the stabilization with post couplers. The frequency of the acceleration (zero) mode TM_{010} in the simulation is to 352.38 MHz.

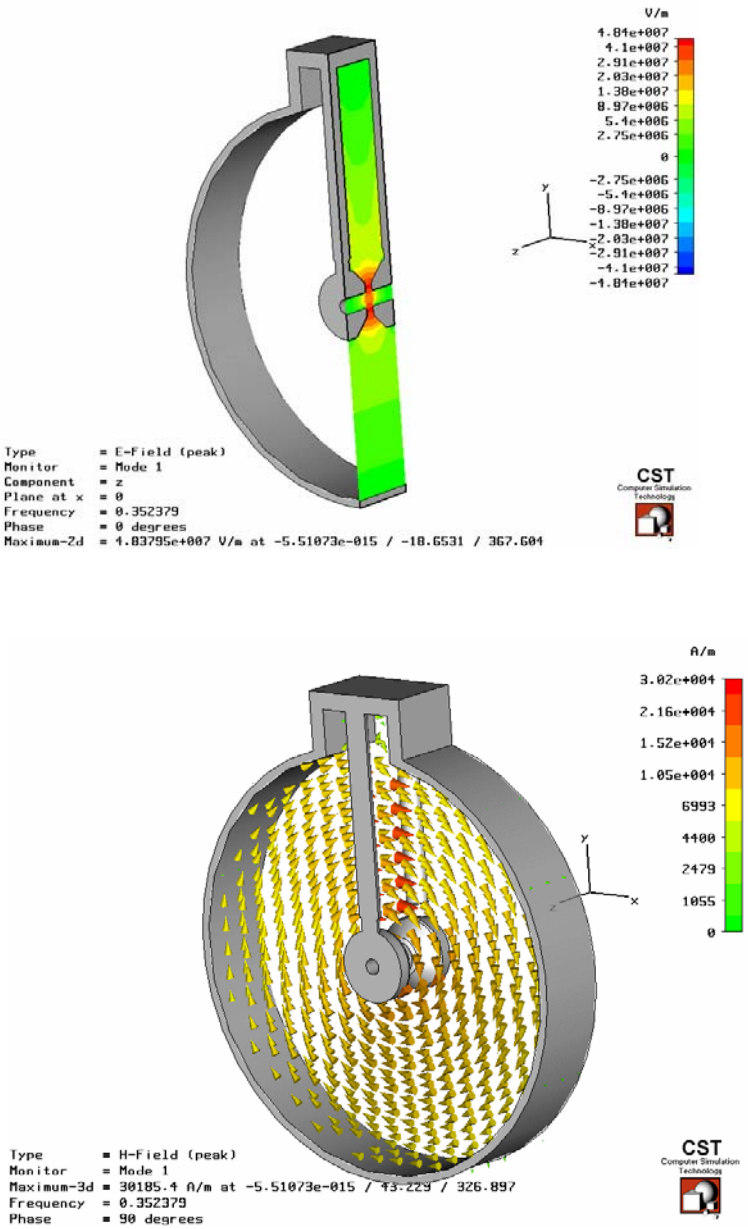

Figure 6: (top) the electric field components in the gap for the acceleration zero mode (TM_{010}) and (bottom) its associated magnetic field

For each additional gap an additional mode is generated and each new device which is inserted into the tank will create a new band containing a number of modes equal to the number of newly created resonant circuits. In the dispersion diagram we plot all modes of all bands in the tank. Since it is too time consuming to simulate the complete tank we limit our

model to nine identical DTL cells with four post couplers as shown in Fig. 7, representing almost one third of tank1.

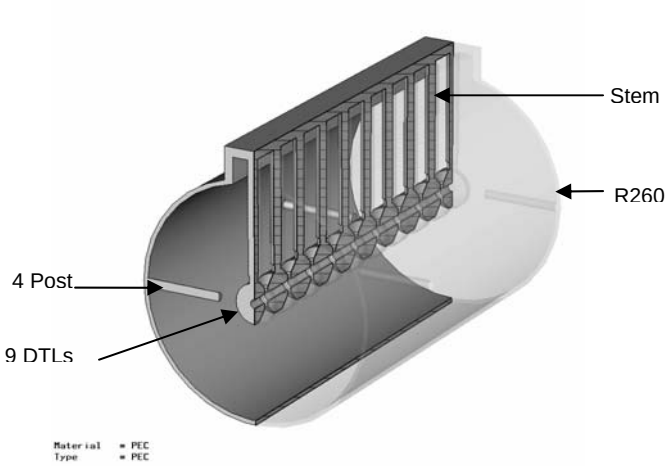

Figure 7: MWS simulation model with nine identical cells four post couplers

To find the post coupler modes we set the boundary conditions in the model (left and right wall) to ideal magnetic. The highest (post coupler zero mode) and lowest mode which define the upper and lower boundaries are shown in Fig. 8. One can see that the direction of the electric field changes but that the amplitude is equal for both modes One can also see that the highest mode (on the left) has no electric field along the gaps, while the lowest mode (on the right) has a certain gap field. The TM_{01} band with the accelerating mode is found with electric boundaries.

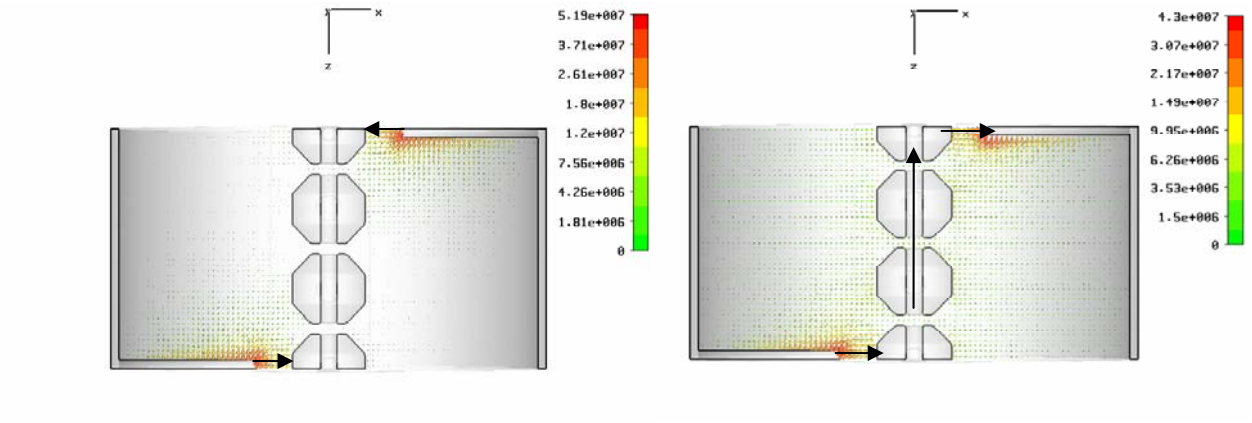

Figure 8: the highest (right) and lowest (left) post coupler modes

Figure 9 shows the dispersion curves for the TM_{01} band, the post coupler band and the band of the drift tube stems. Stabilization occurs when the frequency of the post coupler zero mode is close to the frequency of TM_{010} mode [1, 5]. Reducing the Mode Spacing Area increases the stabilization. It should be noted that in the real tank the highest post coupler mode (zero mode) can not be excited because of the actual (electric) boundary conditions.

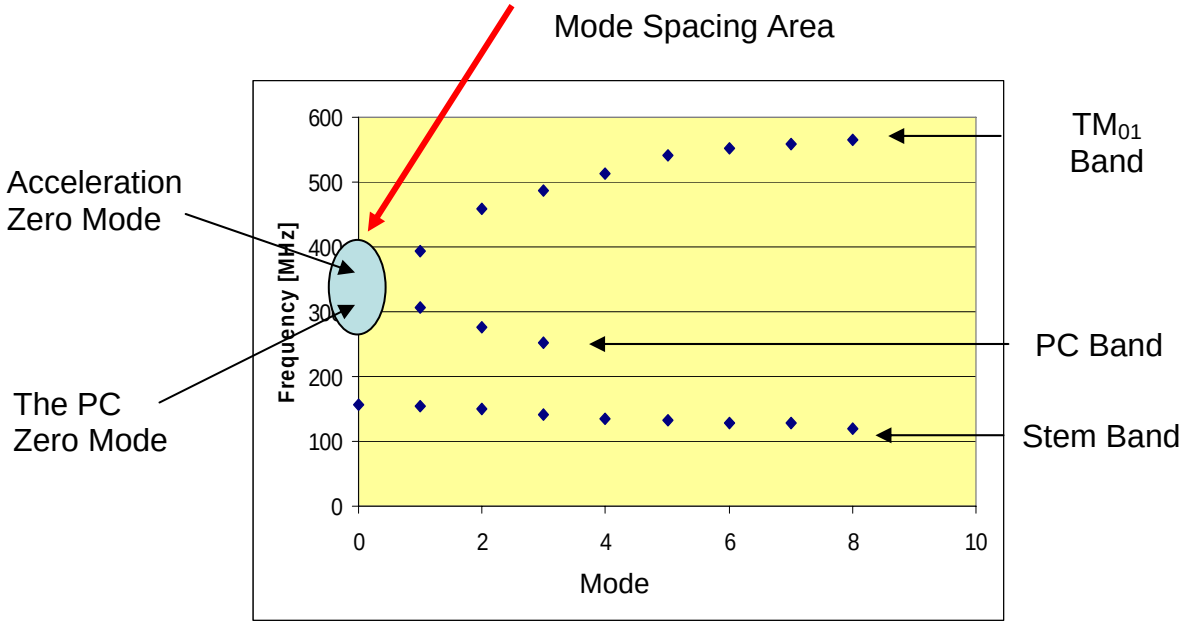

Figure 9: Dispersion curves for nine DTLs, four post coupler and nine (DTL) stems. The bands are TM_{01}, Post Coupler and Stem bands

4- Optimum Post Coupler Length

The post coupler stem represents an inductance while the gap between the post and the drift tube creates a capacitance. Both elements form a resonant circuit whose frequency depends on the length and radius of the post coupler. The capacitance also provides a coupling between the post coupler 0-mode and the accelerating mode which implies that changing the length or radius of the post coupler not only influences the post coupler zero mode but also the acceleration mode as shown in the two graphs of Fig. 10. In the left graph one can see that below stabilization the post coupler acts as a tuner on the frequency of the acceleration mode. From a length of 150 mm onwards the frequency decreases down to the point of maximum stabilization (confluence) and then starts to increase again. In the right graph of Fig. 10 we can see that the frequency of the post coupler zero mode decreases with increasing post coupler length at a rate of ~1.1 MHz/mm. It is thus much more sensitive to changes in the post coupler than the accelerating mode.

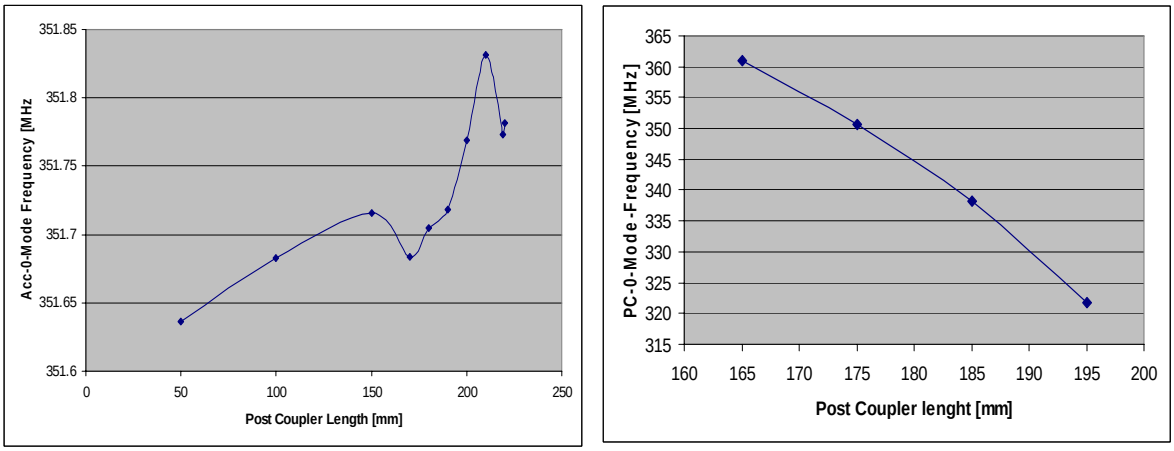

Figure 10: Effect of post coupler length on the acceleration mode (left) and post coupler zero mode (right) using a fixed post coupler radius

For optimum stabilization the post length must be such that the frequency of the post coupler zero mode is close to the operation frequency of 352.2 MHz. Using this criterion we can determine the post length for different radii as depicted in Fig. 11. From this figure we can interpolate the post length for different radii as summarized in Table 2

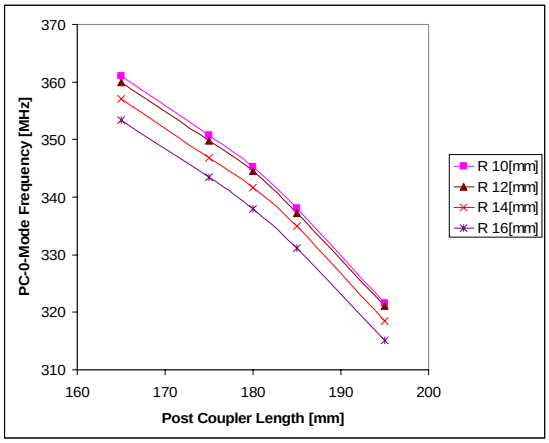

Figure 11: Post coupler length versus post coupler zero mode frequency for different radii

PC Radius [mm]	PC Length [mm]	PCGap [mm]
10	174	41
12	173	42
14	170	45
16	167	48

Table 2: Post coupler length and radius at the stabilization point

5- Optimum Post Coupler Radius

The dispersion curves can also be used to determine the optimum post coupler length for different post coupler radii or vice versa. However, another technique is needed to find the optimum radius for the posts which gives the best stabilisation against frequency errors in the cells. For this purpose we use the tilt sensitivity technique which is usually employed to study post coupler stabilization with mechanical models. First the electric field distribution is measured along the axis for all cells in the simulation model. Then an error is created by changing the drift tube lengths in the end cells giving rise to a frequency shift (±δf) of opposite amplitude (in the order of a few MHz). Finally one measures again the electric field distribution of all cells. From the difference in electric fields one can define the Tilt Sensitivity TS_i for each cell as

$$TS_i = \frac{|E_e|_i - |E_b|_i}{|E_b|_i} \times \frac{1}{\delta f_i} 100\%$$

where $|E_e|_i$ is the electrical field with error for cell *i*, $|E_b|_i$ is the electrical field without error for cell *i* and δf_i is the frequency shift caused by this error.

For our nine unperturbed cells the electrical field distribution along the axis is ideal and all nine electrical amplitudes are equal as shown in the left graph of Fig. 11. The right graph shows the electric field pattern after the introduction of the end cell errors.

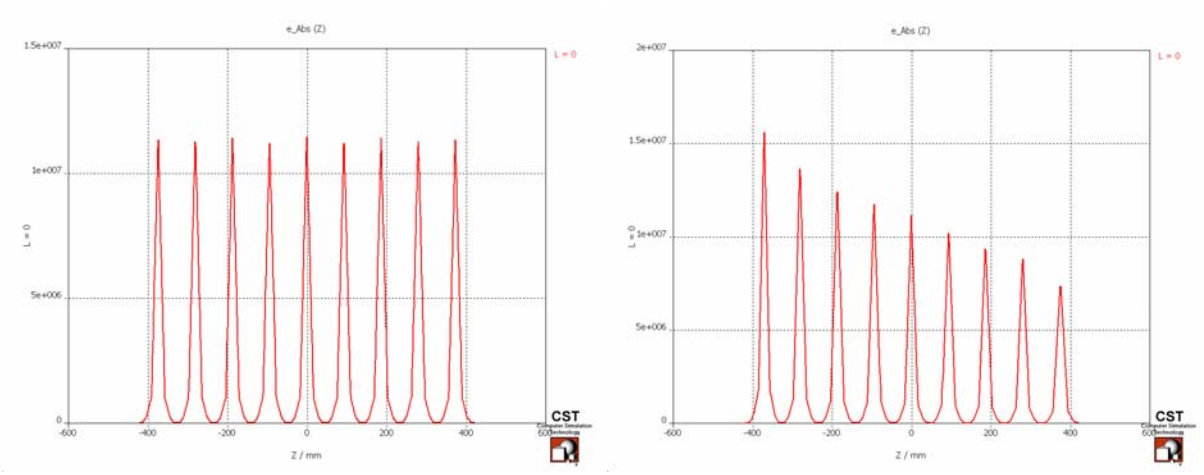

Figure 12: Electric field distribution along the beam axis for nine DTL cells with and without a frequency error in the end cells

The 3D simulation shows a behaviour that agrees well with experimental results [5, 6] which are usually obtained by a bead pull measurement. In the next step we insert the post couplers into the model without removing the error to observe the effect of post couplers on the electric field distribution. Figure 13 shows the effect of the post couplers, whose length and radius have been optimized for maximum stabilization. Plotting the tilt sensitivity versus the cell number (see Fig. 14) before and after the inserting post couplers, we can clearly see a considerable reduction of the slope (note the smaller scale) after the stabilization of the field (excluding the two outermost cells).

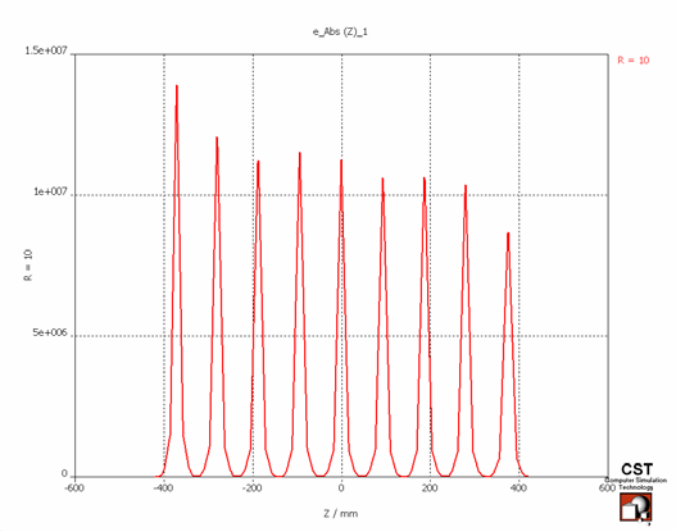

Figure 13: The electrical field distribution along the beam axis after inserting optimized post couplers

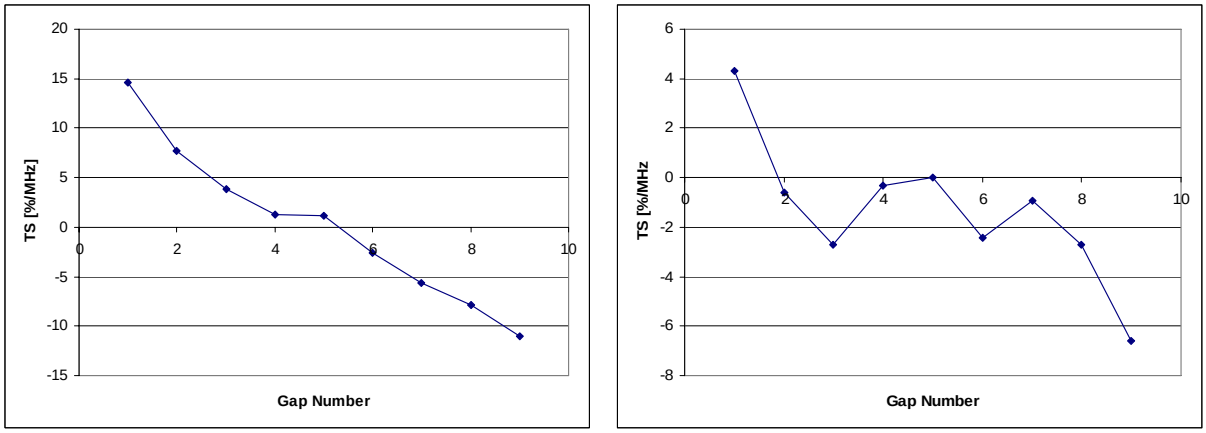

Figure 14: Effect of post couplers on the tilt sensitivity: (left) without post couplers, (right) with post couplers

To find the optimum post radius, we consider the slope of the tilt sensitivity as a measure for the field error inside the tank. Repeating the procedure applied in Fig. 14 for different post coupler radii at optimum post length we can find the optimum post radius for our application. For Tank1, we limit our study to radii between 10 mm to 16 mm in order to keep the mechanics simple, the cooling feasible and the RF losses low. Figure 15 shows the slope of the tilt sensitivity as function of the post coupler radius assuming that the posts are inserted with their optimum length.

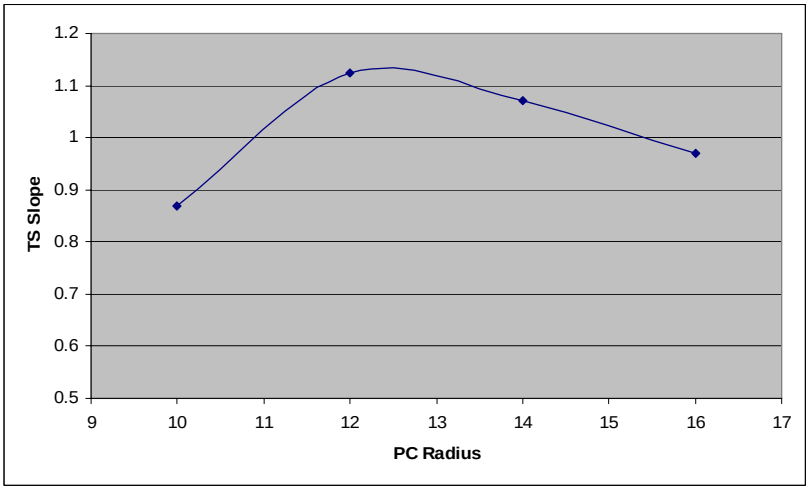

Figure 15: The tilt sensitivity slope as a function of the post coupler radius

Since the smallest slope indicates the best field stabilization we choose 10 mm as the optimum post coupler radius for tank.

6- References

[1] E. Knapp and et al., Stabilization of the Drift Tube Linac by Operation in the π/2Cavity Mode, University of California Los Alamos scientific laboratory, 1967.

[2] P. Lapostolle and A. Septier, Linear Accelerators, North Holland Publishing Company, 1970.

[3] S. Valentinovich Plotnikov *et al*., First section of a 352 MHz Prototype Alvarez DTL tank for the CERN SPL, EPAC06, Edinburgh.

[4] R. Garoby *et al*., Linac4, a new injector for the CERN PS booster, CERN-AB-2006-027, EPAC06, Edinburgh.

[5] S. Machida, Study of the Alvarez Stabilized Post-Couplers, National Laboratory for High Energy Physics, 1985.

[6] M. Vretenar and D. Warner, Field Stabilization in the Quasi-Alvarez Structure, CERN,1990.

Acknowledgements

We acknowledge the support of the European Community-Research Infrastructure Activity under the FP6 “Structuring the European Research Area” programme (CARE, contract number RII3-CT-2003-506395)